Geomechanics and Engineering, *Vol. 35, No. 5 (2023) 555-570*
https://doi.org/10.12989/gae.2023.35.5.555

The role of wall configuration and reinforcement type in selecting the pseudo-static coefficients for reinforced soil walls

Majid Yazdandoust*[1], Amirhossein Rasouli Jamnani[2a] and Mohsen Sabermahani[3b]

[1]*Department of Civil Engineering, University of Qom, Qom, Iran*
[2]*Department of Civil Engineering, University College of Rouzbahan, Sari, Iran*
[3]*School of Civil Engineering, Iran University of Science and Technology, Tehran, Iran*

(*Received November 9, 2022, Revised November 7, 2023, Accepted November 20, 2023*)

Abstract. In the current study, a series of experimental and analytical evaluations were performed to introduce the horizontal pseudo static coefficient (k_h) as a function of the wall configuration and the reinforcement type for analyzing reinforced soil walls. For this purpose, eight shaking table tests were performed on reduced-scale models of integrated and two-tiered walls reinforced by metal strip and geogrid to determine the distribution of dynamic lateral pressure in the walls. Then, the physical models were analyzed using Mononobe-Okabe method to estimate the value of k_h required to establish the dynamic lateral pressures similar to those observed in shaking table tests. Based on the results, the horizontal pseudo static coefficient and the position of resultant lateral force (R) were introduced as a function of the horizontal peak ground acceleration (HPGA), the wall configuration, the reinforcement type as well as maximum wall displacement.

Keywords: pseudo static coefficient; reinforced soil wall; shaking table test; tiered configuration

1. Introduction

Mononobe-Okabe (M-O) method is the common limit-equilibrium method in the pseudo-static analysis that is also widely used for reinforced soil walls. M-O method is a modified version of Coulomb's earth pressure theory in which the effect of a base excitation on retaining walls is simulated by applying the equivalent seismic coefficients in both horizontal and vertical directions to the mass of the potential sliding wedge. Hence, the choice of these coefficients, which can simulate the inertial force induced in the sliding wedge during an earthquake, is an influential factor affecting the accuracy of M-O method.

Various criteria are available for selecting the equivalent seismic coefficients, which are known as pseudo-static coefficients (k_h and k_v). Almost all of them are a function of base excitation parameters and do not take into account the effect of wall characteristics such as wall configuration, reinforcement type, etc. The criterion presented by Choukeir (1995) is one of the few criteria that considers the effect of wall characteristics in calculating the pseudo-static coefficient. In Choukeir's equation, which has been provided for reinforced soil walls with inextensible reinforcements, the effect of wall characteristics has been considered in the form of wall natural frequency as follow

$$k_h = \left[0.5 \Big/ \sqrt{1-\left(\frac{f}{f_n}\right)^2}\right]^{0.5} \times \left[\frac{HPGA}{g}\right] \quad (1)$$

where f, f_n, HPGA are earthquake frequency, wall natural frequency and horizontal peak ground acceleration, respectively. After that, limited and discontinuous studies have been performed to take into account the wall characteristics in determining the pseudo-static coefficients. Hong *et al*. (2005) proposed that $\frac{k_h}{HPGA/g}$ ratio of 0.63 is a proper ratio for steep nailed slopes. In similar study, Leshchinsky *et al.* (2009) suggested this ratio to be 0.3 and 0.4 for reinforced geocell walls and geocell gravity walls, respectively. This ratio was proposed by Huang (2019) for wrap-around geosynthetic-reinforced walls equal to 0.25. Using a series of analytical and experimental studies, Yazdandoust and Ghalandarzadeh (2020) proposed the horizontal pseudo static coefficient as a function of HPGA for integrated steel-strip Mechanically Stabilized Earth (MSE) walls, horizontal grouted nailed walls, and MSE/soil nail hybrid retaining walls.

As mentioned, the choice of pseudo-static coefficient in most existing relationships is based on the base excitation parameters, especially peak acceleration. This is because the acceleration is the main factor of the induced force in the failure mass. Hence, Kramer (1996) suggested that pseudo-static coefficients should be selected based on the Peak Ground Acceleration (PGA). Segrestin and Bastick (1988) proposed a second order polynomial equation to select k_h in MSE walls for HPGA < 0.45g as follow

∗Corresponding author, Assistant Professor
E-mail: M.yazdandoust@qom.ac.ir
[a]Ph.D.
E-mail: rasouly.amirhosein@gmail.com
[b]Associate Professor
E-mail: msabermahani@iust.ac.ir

ISSN: 2005-307X (Print), 2092-6219 (Online)

$$k_h = \frac{HPGA}{g}\left(1.45 - \frac{HPGA}{g}\right) \quad (2)$$

El-Emam (2018) modified Segrestin and Bastick's. equation using a combination of shake table tests and pseudo-static analyzes as follow:

$$k_{h(upp.)} = \frac{HPGA}{g}\left(2.6 - 0.6\frac{HPGA}{g}\right) \quad (3)$$

$$k_{h(low.)} = \frac{HPGA}{g}\left(0.9 - 0.9\frac{HPGA}{g}\right) \quad (4)$$

where $k_{h(upp.)}$ and $k_{h(low.)}$ are the upper and lower bounds for horizontal pseudo static coefficient in geosynthetic-reinforced walls, respectively. Cai and Bathurst (1995) showed that due to the flexibility of MSE walls, the average acceleration of the reinforced mass may be greater than PGA; therefore, the choice of pseudo-static coefficient based on PGA without considering the acceleration amplification along the wall may cause the underestimation of the forces mobilized in the MSE walls. This issue has been considered in CEN (2004) and MOF (2014) for gravity retaining walls by introducing pseudo-static coefficient as a function of the acceleration response along the wall height and the degree of wall flexibility as follow

$$k_h = \frac{1}{r}\left(\frac{a_{Reference}}{g}\right) \quad (5)$$

where r is a variable ranging from 1 to 2, depending on the wall flexibility and $a_{reference}$ is maximum acceleration response at a specified elevation of the wall. Lee *et al*. (2017) suggested that the acceleration amplification issue can be also considered in the definition of pseudo-static coefficient by selecting an average coefficient based on the distribution of pseudo-static coefficients along the wall height.

A literature survey indicates that the effect of wall configuration has not been considered in any of the relationships proposed for the pseudo static coefficient. On the other hand, the effect of reinforcement type has not also been directly included in selecting the pseudo static coefficient in existing relationships. Given the variety of wall configurations and reinforcements used in reinforced soil structures and their influence on wall performance (Zarnani *et al*. 2011, Liu *et al.* 2014, Won *et al.* 2016, Bathurst and Hatami 2020, Samee *et al*. 2021, Kahyaoglu and Sahin 2021, Li *et al*. 2021), it is necessary to provide criteria for selecting the pseudo static coefficients in which the effect of these two important parameters is also considered. Hence, it was attempted in the current study to introduce k_h as a function of wall configuration and reinforcement type using a series of analytical and experimental studies. For this purpose, eight reduced-scale uni-axial shake table tests were performed on integrated and two-tiered wall models reinforced by metal strip and geogrid to determine the distribution of dynamic lateral pressure in the models. Tiered wall models were prepared with three offset distances (D=H/9, 2H/9 and 3H/9) to also take into account the effect of the offset distance in selecting k_h. Then, the physical models were analyzed using Mononobe-Okabe method to estimate the value of k_h required to establish the dynamic lateral pressures similar to those observed in the shaking table tests. Based on the results, the horizontal pseudo static coefficient and the position of resultant lateral force (R) were introduced as a function of the horizontal peak ground acceleration, the offset distance as well as the reinforcement type. Also, using the observed deformations from the physical models, a series of relationships between k_h and the wall deformation were presented.

2. Experimental study

In order to determine the seismic response of the wall models for use in Mononobe-Okabe theory, the shaking table apparatus located at Tehran University was used. The test facility was an uni-axial shaking table device including a servo-hydraulic actuator with the ability to shake specimens at 50 kN with a frequency of up to 10 Hz. In this test facility, a rigid box container with dimensions of 1.82 × 1.23 × 0.8 m was used to prepare the wall models. In order to minimize the unpleasant effect of scaling down models reduction under 1 g conditions, the similitude rules originally proposed by Iai (1989) but as developed by Wood (2004) were used. In the new similitude rules, a correction factor which is a function of soil type is used to correct the original scaling factors. Moreover, the similitude rules provided by Huang (2016) were used to simulate the reinforcements. These similitude rules are presented during the description of the modeling process.

2.1 Preparation of reduced-scaled wall models

In recent years, a large number of tall MSE walls were built for critical applications in earthquake active areas. Although there is no exact criterion for distinguishing these walls from short ones, 6 m has been considered for this purpose in many references (Kongkitkul *et al.* 2010, Liu *et al*. 2014, Jamnani *et al.* 2023). In order to improve the stability and reduce the lateral earth pressure in tall MSE walls, the use of a tiered configuration is proposed as an appropriate solution (Yoo and Kim 2008, Yoo 2018, Safaee *et al*. 2021, Yazdandoust and Bahrami 2022). In this type of configuration, the performance of MSE walls is improved by dividing MSE wall into walls with less height and constructing them on top of each other with considering an offset distance *(D)*. Based on the distance between adjacent tiers, tiered MSE walls (TMSEWs) are divided into three cases according to FHWA (2009) as shown in Figs. 1(a)-1(c). In the first and second cases, the tiers behave in an integrated and independent manner, respectively. But, the offset distance in the third case is in the range that causes an interaction between the upper and lower tiers ($(H_1+H_2)/20 \leq D \leq H_1.tan(90-\phi)$, where H_1 and H_2 are the heights of the lower and upper tiers, respectively, and ϕ is the internal friction angle). Given the complex behavior of the third case of tiered walls and the need for further study on their behavior (Hosseininia and Ashjaee 2018), the current study focused on this case of tiered walls. For this purpose, the offset distance range was chosen such that the models could

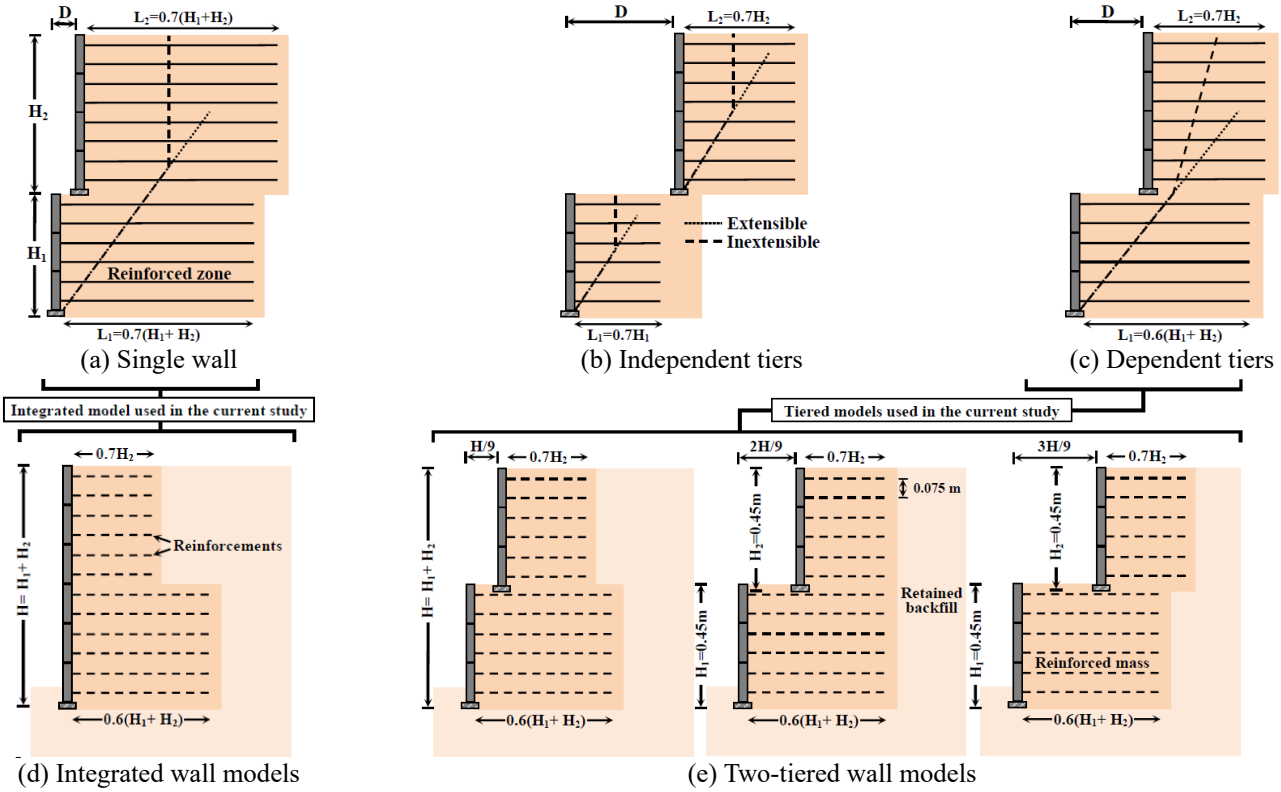

Fig. 1 Classification of two-tiered MSE walls and configuration of the models used

be classified in the third category of TMSEWs. Considering the friction angle of soil used (~38°), the minimum and maximum offset distances required for the wall models to be classified in the third category were H/20 and $1.28H_1$, respectively. Hence, the tiered wall models were constructed in two tiers of the same height ($H_1=H_2=H/2=0.45m$) and three offset distances ($D=H/9, 2H/9, 3H/9$), as shown in Fig. 1(e). These models were equivalent to real two-tiered walls with a height of *9* m.

Based on the recommendation provided by FHWA (2009) to prevent the tiers from sliding, 0.06 m and 0.03 m were selected as the embedment depth for lower and upper tiers, respectively. A 0.2-m thick foundation was also considered to provide real conditions for occurring possible settlements and the lateral sliding. On the other hand, according to the FHWA guidelines, the length of reinforcements located in the lower and upper tiers were selected to be $0.6(H_1+ H_2)$ and $0.7H_2$ in all models, respectively. In addition to the tiered wall models, an integrated configuration was also used for comparison with the tiered models. To construct the integrated wall models, the wall height, the subsoil thickness and the reinforcement arrangement were considered to be the same as for the tiered models. This produced an integrated wall with uneven reinforcement lengths, as seen in Fig. 1(d). Because the arrangement chosen for the reinforcements in the integrated model did not follow the FHWA guidelines, the stability of the integrated models was evaluated under both static and dynamic conditions to ensure the accuracy of the design using the limit equilibrium method, FE analysis and FHWA guidelines. Analyzes showed that the minimum safety factor in both integrated and tiered wall models was related to the external stability and that integrated wall models have acceptable stability. The minimum safety factors calculated for each model under static and dynamic conditions are presented in Table 1. The geometry of the physical models is also summarized in Table 2.

A silica sand with a mean diameter (D_{50}) of 0.285 was used at a relative density (D_r) of 85% to construct the body of models. This soil material, called Firuzkooh #161 sand, was a synthetic soil composed of angular particles with a specific gravity of 2.66 and a fines content of about 6% that had the maximum and minimum dry unit weights of 16.6 kN/m^3 and 14.6 kN/m^3, respectively. Based on the results of consolidated-drained triaxial tests at confining stresses equivalent to the pressures induced in the physical models (5~15 kPa), peak and post-peak friction angle were 44°-47° and 38°-41°, respectively. An apparent cohesion of about 4 kPa was also observed in the results, which can be attributed to soil moisture and surface tension formed in the soil specimens. It can be seen in the triaxial test results that the stiffness of the soil at a confining stress equivalent to the pressure induced in the models was 3.4-3.8 times less than that at a confining stress equivalent to the pressure induced in the prototype. This ratio was similar to that proposed for soil stiffness in a 1g model with a geometric scaling factor of 1:10 ($E_{S(Prototype)} = (N)^{\lambda}E_{S(Model)}$; where E_S is soil elastic modulus and λ is a correction factor which is recommend to be 0.5 for cohesion less soils).

Because steel-strip and geogrid are the most common reinforcements used in reinforced soil walls, these two reinforcements were chosen to reinforce the wall models.

Table 1 The values of safety factor related to the external stability for the models under static and dynamic conditions

Reinforcement type	Wall configuration	Offset distance	Safety factor					
			Static conditions			Seismic conditions		
			FHWA	LE [(b)]	FE [(c)]	FHWA	LE [(b)]	FE [(c)]
Metal strips	MS-D=0	0 [(a)]	2.113	2.085	1.655	1.872	1.492	1.585
	MS-D=H/9	H/9	2.352	2.289	1.915	1.995	1.620	1.763
	MS-D=2H/9	2H/9	2.618	2.551	2.117	2.204	1.813	1.921
	MS-D=3H/9	3H/9	2.825	2.770	2.358	2.415	1.910	2.108
Geogrid	G-D=0	0 [(a)]	1.805	1.758	1.441	1.625	1.201	1.258
	G-D=H/9	H/9	1.978	1.887	1.623	1.827	1.441	1.505
	G-D=2H/9	2H/9	2.198	2.034	1.801	2.005	1.605	1.691
	G-D=3H/9	3H/9	2.326	2.283	1.951	2.115	1.705	1.768

[a] Integrated wall model; [b] limit equilibrium method; [c] Finite elements analysis

Table 2 Geometry of the physical models

Wall model	Wall configuration	Reinforcement type	Upper tier		Lower tier		S_H [a] (m)	S_V [b] (m)
			L_2 (m)	H_2 (m)	L_1 (m)	H_1 (m)		
MS-D=0	Integrated	Metal strips	$0.7H_2$	0.45	$0.6(H_1+H_2)$	0.45	0.075	0.075
MS-D=H/9								
MS-D=2H/9	Tiered							
MS-D=3H/9								
G-D=0	Integrated	Geogrid	$0.7H_2$	0.45	$0.6(H_1+H_2)$	0.45	----	0.075
G-D=H/9								
G-D=2H/9	Tiered							
G-D=3H/9								

[a] Horizontal spacing of reinforcements; [b] Vertical spacing of reinforcements

As suggested by Viswanadham and Mahajan (2007) and Safa *et al.* (2019), these reinforcements were scaled down by considering the tensile stiffness and the soil-reinforcement interaction as two influential factors. Using Huang's 1 g similitude rules for tensile stiffness ($(E_{st})_{prototype}=N(E_{st})_{model}$ for strip reinforcements and $(E_{sh})_{prototype}=N^2(E_{sh})_{model}$ for sheet reinforcements) and the pullout resistance ($(P_R)_{prototype}=N^2(P_R)_{model}$ for strip reinforcements and $(P_R)_{prototype}=N(P_R)_{model}$ for sheet reinforcements), a series of the uniaxial tensile and pull-out tests were carried out to determine the best substitute for steel-strip and geogrid in reduced-scale models. Moreover, the opening size was also considered as a criterion to select the geogrid. For this purpose, the Yoshida and Tatsuoka criterion was used. Yoshida and Tatsuoka (1990) proposed that s_t/D_{50} should be greater than 10, where s_t is the spacing between the transverse ribs of the geogrid and D_{50} is the mean diameter of the soil aggregate. The global reinforcement stiffness (S_{global}) was another important factor that was also used to control the accuracy of scaling down the reinforcements. This factor is the main parameter in the *Stiffness Method* (Bathurst and Naftchali 2021) and expressed as

$$S_{global}=\frac{\sum_{i=1}^{n}J_i}{H} \quad (6)$$

where J_i is the tensile stiffness of the i^{th} reinforcement layer expressed in units of force per unit width of wall and H is the wall height. Based on Eq. (6), the values of S_{global} for the metal-strip reinforced-soil wall models at small and real scale were calculated to be 4921.37 and 49953.1 kN/m^2 and for the geogrid-reinforced soil wall models at small and real scale were calculated to be 269.79 and 2783.58 kN/m^2. A comparison of $S_{global(Prototype)}/S_{global(Model)}$ ratio for each model with that calculated using the similitude law ($S_{global(Prototype)}=N.S_{global(Model)}$) verified the reinforcement simulation and showed that reduced-scale models had internal global stiffness such as would be expected at prototype scale. The physical and mechanical properties of the reinforcements at real and reduced scale are presented in Table 3.

Despite the use of two different types of reinforcement, the same facing type was used for all models in order to eliminate the effect of facing type on the results. For this purpose, cruciform concrete panels with dimensions of 0.15 × 0.15 × 0.015 m were selected that had been

Table 3 Properties of metal strip and geogrid used in scale of prototype and model

Index properties	Metal strip		Geogrid	
	Prototype	Model	Prototype	Model
Material	Steel	Phosphor Bronze	PVC coated Polyester yarns	Polypropylene
Thickness [mm]	4.0	0.4	2.00	0.90
Longitudinal and transverse rib width, b_l, b_t [mm]	50,---	5.0,---	11, 2.5	0.90, 0.6
Longitudinal and transverse opening size, $s_l \times s_t$ [mm]	---	---	25×35	7.5×7.5
Elongation at ultimate tensile load, ε_u [%]	0.37	0.46	6.08	6.28
Secant tensile stiffness per unit wall width at ε_u, J [kN/m]	36216	356.8	2018.1	19.56
Pullout resistance under σ_v=70[a],7 [b] kPa, R_p [kN/m/m][c]	9.58	0.93	155.85	14.75
Pullout resistance under σ_v=140[a],14[b] kPa, R_p [kN/m/m][c]	11.93	1.20	219.6	21.37
Pullout displacement under σ_v=70[a],7[b] kPa, $d_{pullout}$ [mm]	4.75	0.57	14.2	2.90
Pullout displacement under σ_v=140[a],14[b] kPa, $d_{pullout}$ [mm]	3.55	0.43	14.5	2.67

[a]:for prototype; [b]: for model; [c]: force per unit reinforcement length per unit wall width

scaled down based on the flexural strength criterion ($(M)_{prototype} = N^3(M)_{model}$) and flexural tests as reported by Samee *et al.* (2022). To connect the model geogrid with concrete panels, a special connector was used as recommended by Bathurst (1990). This connector, which is presented in Fig. 2(a), consisted of two metal strips that the geogrid was placed between them and their assembly was connected to the concrete panel through the tie strips cast buried in the panel.

In order to achieve a reliable simulation of the prototype, the construction sequence of actual integrated and tiered walls was exactly simulated in the construction procedure of the models. To construct the body of models, the soil was loosely placed into the box container at a water content of 6% in 0.05 m lifts (equivalent to 0.5-m lifts in the prototype MSE walls (FHWA 2009), and was compacted using the hand tamper to reach a desired thickness (0.0375 m). This method, called the volume-controlled method, is a common form of preparing physical models (Komak Panah *et al.* 2015, Lee 2019, Safaee *et al.* 2020, Altay *et al*. 2021, Jin *et al.* 2021, Yazdandoust *et al*. 2022, Mollaei *et al.* 2022, Yadegari *et al*. 2023). This procedure was verified by placing five 50 mm-diameter compaction cylinders within each lift before compaction, to sample the soil relative compaction at different locations, by measuring the bulk unit weight of compacted soil in each cylinder. Just as lighter compaction is done near the wall face in practice, the soil behind the panels was more lightly compacted than the reinforced mass. The relative density of this zone was about 65%. It should be noted that horizontal and vertical layers of black-colored sand was poured close to the front of the container during construction to allow better detection of shear band development. The pictures of finished the wall models in the perspex container are given in Fig. 3.

2.2 Instrumentation and base excitations

The determination of the force mobilized in the reinforcements was the most important goal of the laboratory study phase in the current research. For this purpose, four rows of reinforcements were selected at different elevations to measure the force mobilized along them, as shown in Fig. 3. The force mobilized along each reinforcement was measured by attaching four strain gauges to its surface (Figs. 2(b) and 2(c)). Because the width of

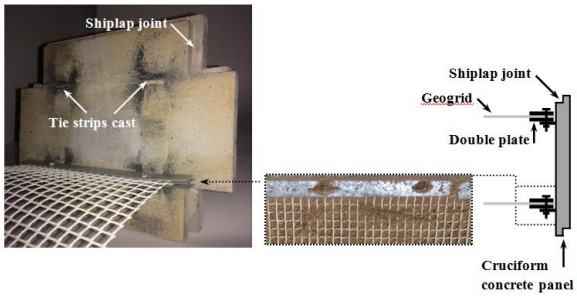

(a) Detail of connector used to connect the model geogrid with concrete panels

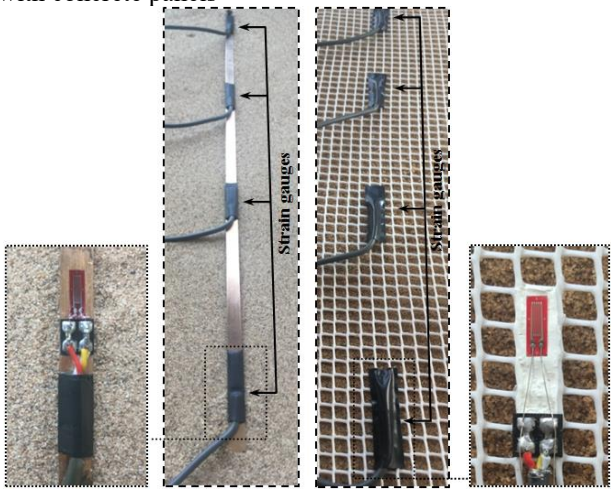

(b) Position of strain gauges attached to strips (c) Position of strain gauges attached to geogrid

Fig. 2 The reduced scale facing panel and reinforcements

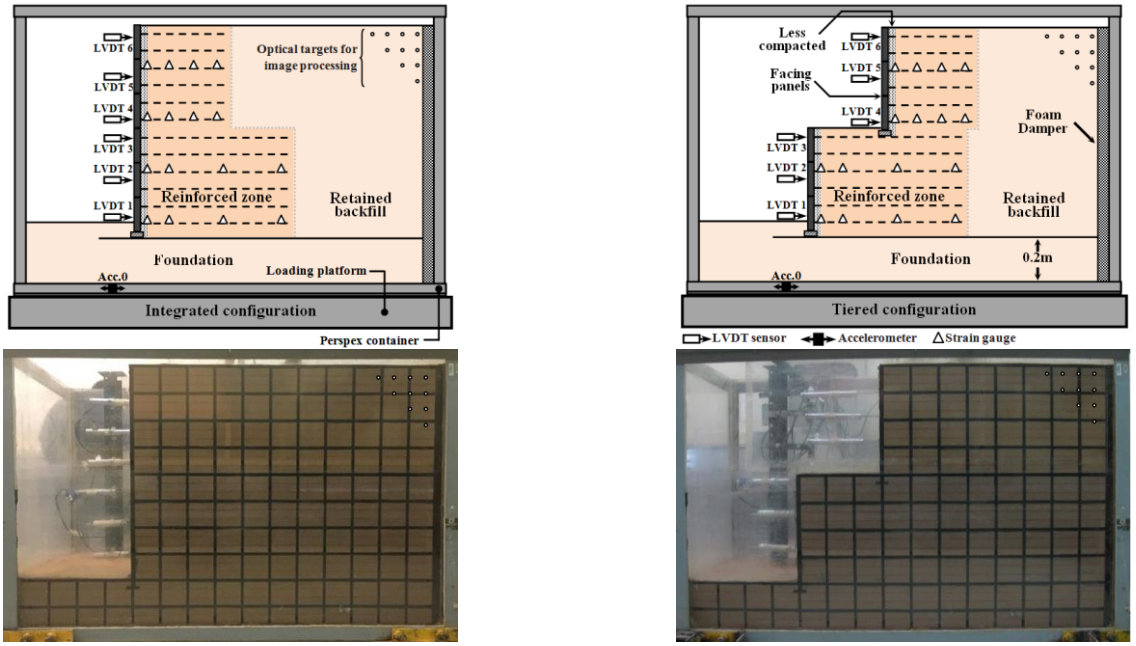

(a) integrated wall model (b) two-tiered wall model with an offset distance of 3H/9

Fig. 3 The picture and instrumentation of the models

geogrid ribs was insufficient for attaching the strain gauges, 5 consecutive apertures were filled by melting the geogrid base material to provide the necessary width for the installation each stain gauge, as shown in Fig. 2(c). The use of this method instead of installing the Teflon foil strips, which has been recommended by Viswanadham and König (2004) and is very common, can greatly prevent the local increase in geogrid stiffness. However, in both these methods, the local strain as measured by the strain gauge will not represent the global strain over one or more apertures of the geogrid. This defect can be corrected using a calibration factor (CF = the ratio of the global strain to local strain) that was measured to be 1.09 for the model geogrid. This factor reported to be 1.29 to 1.7 for geogrids instrumented with foil-type strain gauges (Allen and Bathurst 2014, Jiang *et al*. 2016). On the other hand, a relationship was also obtained for each of the reinforcement used in the current study to convert the axial strain of the reinforcement into the axial force mobilized in it. These factors were determined using a series of axial tensile tests on the instrumented metal strip and geogrid by a strain gauge. Moreover, six LVDTs (linearly variable differential transformer) were also used at different elevations of the models to measure the horizontal movements at different heights during seismic loading, as illustrated in Figs. 3(a) and 3(b). An accelerometer was also mounted on the box container to measure the input acceleration. On the other hand, the particle image velocimetry (PIV) technique was utilized to identify the failure mechanism in the models.

The PIV technique, which has been used extensively in geotechnical studies (Lee *et al*. 2021, Seo *et al*. 2021), is a non-invasive method for accurate measurement of shear strains within the soil mass by following the movement of 'patches' of soil in sequential images. This technique was employed for the first time by White and Take (2002) to identify the critical failure surface in the soil mass. In order to generate the considerable data for image processing, a charge-coupled device (CCD) camera was employed to take digital images of models before and after each stage of testing.

Variable-amplitude harmonic excitations were used to shake the models. This type of excitation is more similar to a real earthquake than harmonic motions with constant amplitude (Hatami and Bathurst 2000). These excitations were applied in the sequential steps in which the duration was constant (equal to 13 s) and the peak acceleration was increased from 0.5 g in increments of 0.1 g at each step until failure occurred. In order to avoid the occurrence of resonance in the models, a frequency of 5 Hz was chosen for input motion because it was sufficiently distant from the natural frequencies measured for each model during the free-vibration tests. The measured natural frequencies of the models ranged between 9.8 to 26.2 Hz. According to the similitude law for frequency in cohesion less soil ($f_{prototype} = 1/N^{1-\lambda/2}.f_{model}$), the frequency selected for the input motion corresponded to the predominant frequency of real excitation at approximately 1 Hz.

2.3 Shaking table test results

To verify Mononobe-Okabe (M-O) theory with the physical models, the force mobilized in the reinforcements was used as the main criterion (El-Emam 2018, Huang 2019, Xu *et al*. 2020). In addition to force, the displacement was also used to verify the analytical methods based on the performance (Macedo and Candia 2020, Lee *et al*. 2021). Hence, among all the results obtained from the shaking table tests, only the failure mechanism, the force mobilized

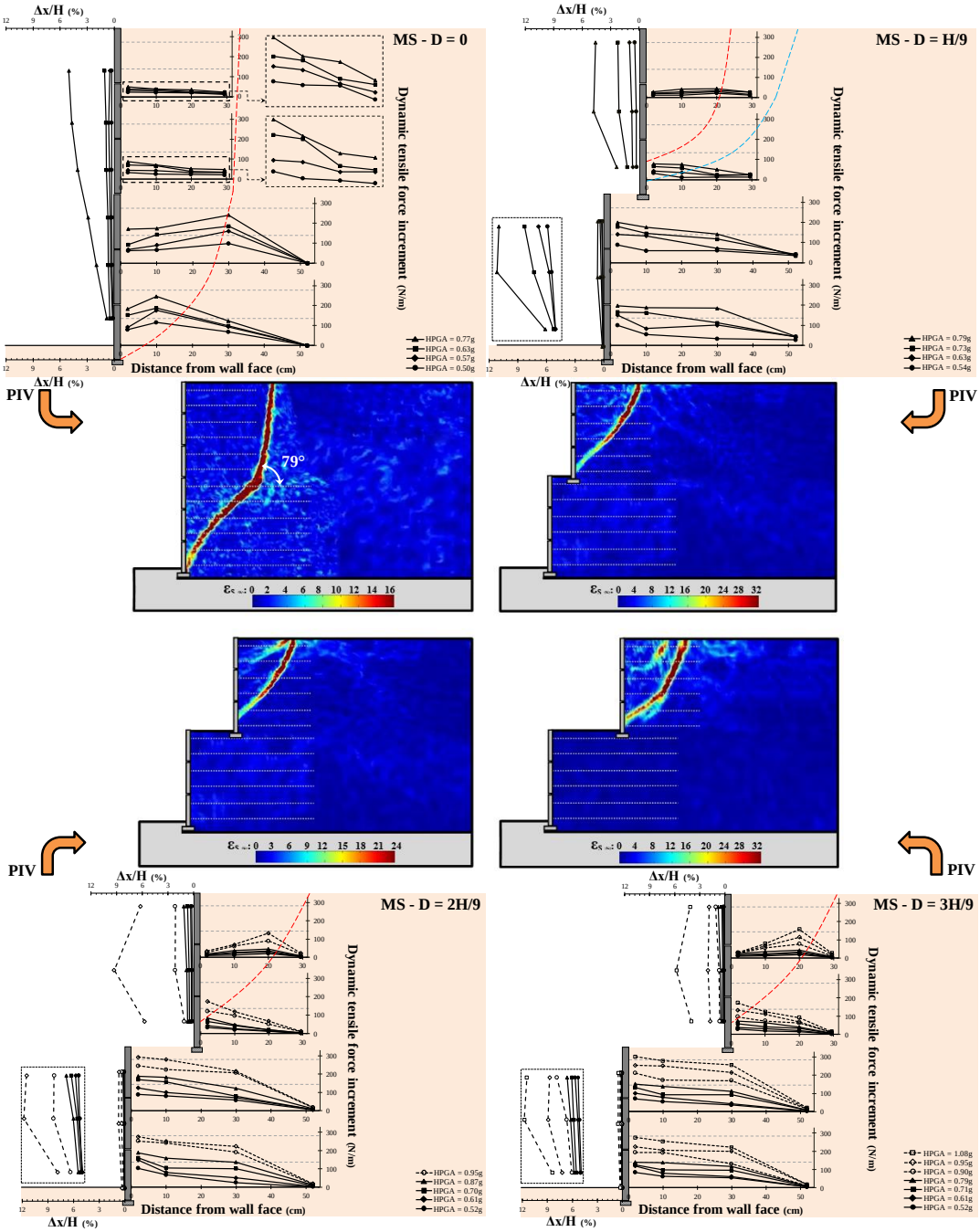

Fig. 4 Distributions of tensile forces along reinforcements, lateral displacement profiles and PIV results for walls reinforced by metal strips

in the reinforcements and the lateral wall movement are described and disused here.

2.3.1 Failure mechanism

The propagation of cumulative shear strain (ε_s) obtained by PIV technique in the last shaking step is presented in Figs. 4 and 5 for the models reinforced by metal strips and geogrid, respectively. In contrast to those predicted by the FHWA guidelines, the failure surfaces only formed in the upper tier when using a two-tiered configuration, while the slip surfaces developed along the wall height in the integrated wall models. This means that the use of a tiered configuration in the MSE walls, even with a small offset distance, reduces the penetration depth of the failure surface and prevents it from developing in the lower tier.

In integrated wall models, the failure mechanism consisted of an internal failure and an external failure that appeared as a curve in the lower half and as an inclined line in the upper half of the wall. The occurrence of external failure in the upper tier can be attributed to the short length and low pullout resistance of the reinforcements in this zone. This short length, which was about half the length recommended for MSE walls, prevented the reinforcements from acting as an anchoring mechanism and minimized the

contribution of the upper reinforcements to the stability of the wall. As a result, an active zone comprised of reinforcements formed in the upper half of the wall and was separated from the intact soil by an inclined plane of a specific angle. The horizontal angle of the inclined line was measured to be about 79° and 75° in the metal-strip and geogrid reinforced wall models, respectively, while it was 58° for both reinforcement types in the FE analysis. Considering that the angle of external failure is defined as a function of the post-peak friction angle of the backfill soil (Kumar and Rao 1997, Tufenkjian and Vucetic 2000, Tatsuoka *et al*. 2012) and the post-peak friction angle of the soil was also about 38°, the horizontal angle of external failure in the integrated wall models can be introduced in the form of $A_0\left(\frac{\varphi_{post-peak}}{2}+\frac{\pi}{4}\right)$. In this relationship, A_0 can be considered equal to 1.23 and 1.17 in the wall models reinforced by metal strip and geogrid, respectively. A change in the reinforcement type led to a change in the geometry of internal failure. This geometric change from a convex plane in the geogrid-reinforced model to a concave plane in the metal-strip reinforced model was related to the reinforcement stiffness and has been also reported by Komak Panah *et al*. (2015) and Yazdandoust (2017).

In tiered wall models, an internal failure plane was detected in the reinforced zone of the upper tier that started from behind the topmost layer of reinforcement and developed through the reinforcement layers toward the lower one-third of the wall facing. This failure plane, which was unchanged for both types of reinforcement as the offset distance changed, was more convex than that for the geogrid-reinforced models because of the more extensibility of the geogrid. An external failure surface also formed in the geogrid-reinforced models with a slight delay after the formation of the internal failure plane. The external failure started from the backfill surface and developed toward the toe of the upper tier in the form of a composite surface including a convex plane and an inclined planar surface. This external failure, which developed further with increasing offset distance, can be attributed to the active state in the backfill caused by significant outward movement occurred in the upper tier. As seen in Fig. 4, a series of incomplete failure surfaces also formed within the failure wedge in the metal-strip tired walls with long offset distance (*D=2H/9* and *3H/9*) after the occurrence of the main failure surface. These failure surfaces, which were due to the continuation of seismic loading after the occurrence of the main failure plane, reject the hypothesis of the rigidity of the failure wedge in analytical methods for MSE walls.

2.3.2 Force distribution along reinforcements

The distribution of tensile force along the reinforcements at different values of HPGA for models reinforced by metal strips and geogrid are presented in Figs. 4 and 5, respectively. As can be seen in all models, the distribution of the axial forces along the reinforcements delineated a triangular shape with a certain maximum point (T_{max}). Matching the failure surfaces obtained from the PIV technique with the force distribution in the reinforcements showed that the location of T_{max} will be approximately at the intersection of the failure surface with the reinforcements if the shear bands can be localized and, consequently, the failure plane is formed. Otherwise the maximum tensile force is mobilized at reinforcements' head (the position of the connection with the facing). It means that in reinforced soil walls where it is not possible to localize the shear bands and the wall experiences only a simple shear deformation along horizontal planes, the position of connecting reinforcements on the facing as the place of mobilization of the maximum force should be given special attention. The lack of localizing the shear bands in the lower half of the wall was observed when using a tiered configuration in the models. Increasing the density of reinforcements in the reinforced mass was another factor preventing the localization of shear bands as reported by Koseki *et al*. (1998). It is also observed that the magnitude of T_{max} increased in all models by decreasing the elevation of reinforcement rows and increasing HPGA value. This finding emphasizes the importance of paying more attention to reinforcements located in the bottom rows as critical reinforcements under seismic conditions. The generation of T_{max} at the intersection of the failure surface with the reinforcements and increasing its value in bottom rows was also reported by Watanabe *et al*. (2003), Stuedlein *et al.* (2010), Huang (2019) and Yazdandoust (2018) for geosynthetic and metal-strip reinforced-soil walls. The reduction in reinforcement load due to the use of geogrid was another point that can be seen in Fig. 5. This reduction, which was mostly seen in the lower half of the walls and was accompanied by a change in the failure geometry from concave to convex in the lower half of the integrated walls and also the formation of an external failure surface in the upper half of the tiered walls with a slight delay after the formation of the internal failure plane, can be considered as an advantage to prevent the concentration of force in the lower reinforcement layers and consequently the concentration of lateral pressure in this part of the wall.

For better understanding this issue, the distribution of normalized lateral pressure increment ($\Delta\sigma_{dyn}/\gamma H$) along the wall height is also presented in Fig. 6 during the experience of different base accelerations. The lateral pressure value at the depth corresponding to each reinforcement layer $(\Delta\sigma_h)_I$ was converted from the measured reinforcement force using the following equation.

$$(\Delta\sigma_h)_i = \frac{\Delta T_{\max,i}}{S_V \times S_H};\ where\ S_H = 1\ in\ sheet\ reinforcements \tag{7}$$

where S_V and S_H are the vertical and horizontal intervals of reinforcements, respectivly, and $\Delta T_{max,i}$ is the maximum force mobilized at i*th* reinforcement layer. The use of mobilized force in reinforcements to determine lateral pressure is a common method that has been used in many studies (Bathurst 1990, Krishna and Latha 2011, Yazdandoust 2018, Huang 2019). The comparison of models showed that the use of a tiered configuration had a significant effect on reducing the dynamic lateral pressure.

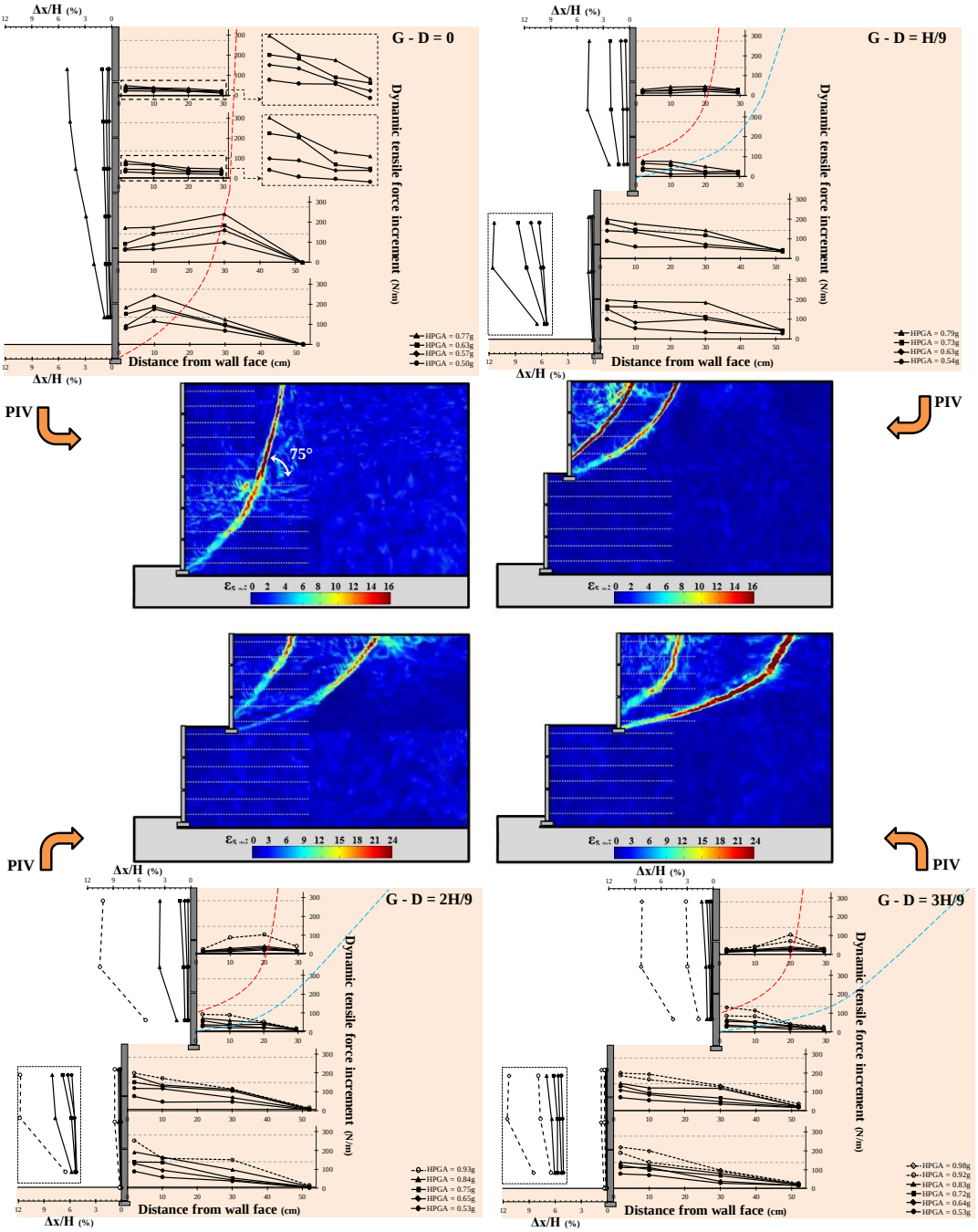

Fig. 5 Distributions of tensile forces along reinforcements, lateral displacement profiles and PIV results for walls reinforced by geogrid

This effect, which was more evident in the lower half of the models and was more pronounced in the models reinforced by metal strips, became more even noticeable with increasing the offset distance and the base input acceleration. As can be seen in Fig. 6, using a $D = H/9$ in the models reinforced by geogrid resulted decreasing $\Delta\sigma_{dyn}/\gamma H$ by about 3-10% in the upper tier and about 10-19% in the lower tier, while these reductions reached about 8-15% and 18-26% in the upper and lower tier of the metal-strip reinforced models, respectively. It means that the effect of using a tiered configuration on reducing the lateral pressure of the lower tier was approximately 2.2 times that of the upper tier. With increasing the D/H ratio to 0.33, the reduction of $\Delta\sigma_{dyn}/\gamma H$ in the lower tier of tiered walls reached about 30-43% and 48-55% in the wall models reinforced by geogrid and metal strip, respectively. This difference indicated that the use of extensible reinforcements diminishes the effect of using a tiered configuration on reducing dynamic lateral pressure.

2.3.3 Lateral wall displacement

The lateral displacement profiles at different shaking intensities are presented in Fig. 7. Comparison of integrated and tiered wall models shows that the use of a tiered

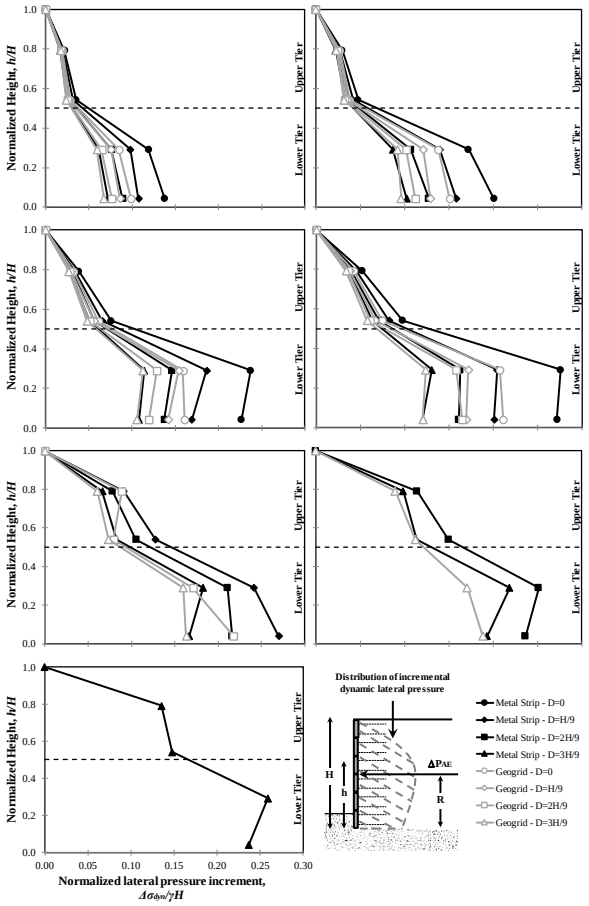

Fig. 6 Distribution of normalized lateral pressure increment along the wall height under different base excitations

configuration allowed each tier to behave independently.

This is not accordance with that predicted by the FHWA (2009) for tiered MSE walls with intermediate offset distances (the third case). The failure to consider seismic conditions for tiered walls in the FHWA guidelines can be the main reason for this discrepancy. As seen, the independent performance of tiers caused two different effects to be observed in the upper and lower half of the wall due to use the tiered configuration. In the lower half of the wall, considering an offset distance of H/9 decreased the lateral deformations while it led to a significant increase in the deformation of the upper half. This increase can be attributed to the discontinuity between the upper and lower tier. Because the upper half of the walls experienced a higher level of acceleration, separating upper tier from the lower half allowed it to react more freely to excitations, and consequently, led to increase the lateral displacements in this part of the walls. As seen in displacement profiles, this increase was mitigated by using a sufficiently large offset distance. This can be clearly seen in Fig. 8, where the excess movement caused by the use of a tiered configuration declined sharply in the upper tier when the offset distance exceeded *2H/9* for both reinforcement types.

This means that the minimum offset distance required to neutralize the negative effect of a tiered configuration on the movement of the wall crest is *2H/9*. Hence, *0.22H* can be introduced as the minimum offset distance required when constructing MSE walls in a two-tiered configuration.

The displacement profiles also show that the use of inextensible reinforcements can have a significant impact on reducing the lateral deformation of tiered walls, especially during the experience of high levels of base acceleration. This impact, which was also seen in integrated walls, was much more pronounced in tiered walls and was more often seen in the upper tier. In order to better understand the simultaneous effect of a tiered configuration and reinforcement type on the displacement response of models under different seismic conditions, the variation of maximum normalized wall deflection ($D_{max}= \Delta x_{mas}/H$) versus *D/H* ratio in different base accelerations is presented in Fig. 8 for each tier separately. As can be seen, the influence of reinforcement type on D_{max} was more evident at smaller *D/H* ratios and larger base accelerations. In integrated walls, the effect of using inextensible reinforcement in reducing the lateral deformation was more observed in the lower half of the wall while this effect was more evident in the upper tier of tiered walls. Due to the fact that moving the upper part of walls has a greater impact on the performance of structures located on the walls, it can be concluded that the use of inextensible reinforcements in the walls to control the behavior of these structures is more effective in tired walls. It was also observed in Fig. 8 that the influence of base acceleration magnitude and reinforcement type on D_{max} gradually fades by constructing the tiered walls with larger offset distance. This, which was more prominent in the lower tier, means that the use of a large enough offset distance can be an effective solution in optimal design of tiered walls located in high seismic risk areas and projects in which there are some application restrictions on selecting the type of reinforcement.

3. Analytical study

Mononobe-Okabe method (M-O) was used to analysis the wall models tested by shaking table. M-O method, which is a seismic developed version of Coulomb's earth pressure theory, simulates the effect of a base excitation on retaining walls in the form of dynamic active and passive forces (P_{AE} and P_{PE}) by applying the equivalent seismic coefficients (k_h and k_v) to the mass of the potential sliding wedge in both horizontal and vertical directions as follow

$$\begin{pmatrix} P_{AE} \\ P_{PE} \end{pmatrix} = \frac{1}{2}\gamma H^2(1-k_v)\begin{pmatrix} K_{AE} \\ K_{PE} \end{pmatrix} \tag{8}$$

$$\begin{pmatrix} K_{AE} \\ K_{PE} \end{pmatrix} = \frac{cos^2(\varphi \mp \theta - \beta)}{cos^2\theta . cos\beta . \cos(\delta \pm \theta + \beta)\left\{1 \pm \sqrt{\frac{\sin(\delta+\varphi).\sin(\varphi \mp \alpha - \beta)}{\cos(\delta \pm \theta + \beta).\cos(\theta - \alpha)}}\right\}^2} \tag{9}$$

where K_{AE} and K_{PE} are the dynamic active and passive pressure coefficient, respectively. β is $tan^{-1}\frac{k_h}{1-k_v}$. γ, φ, δ, θ and α are the soil unit weight, the internal friction angle of soil mass, the friction angle at soil-facing interface, the wall slope angle from the vertical and the backfill slope angle, respectively. Seed and Whitman (1970), Bathurst and Cai

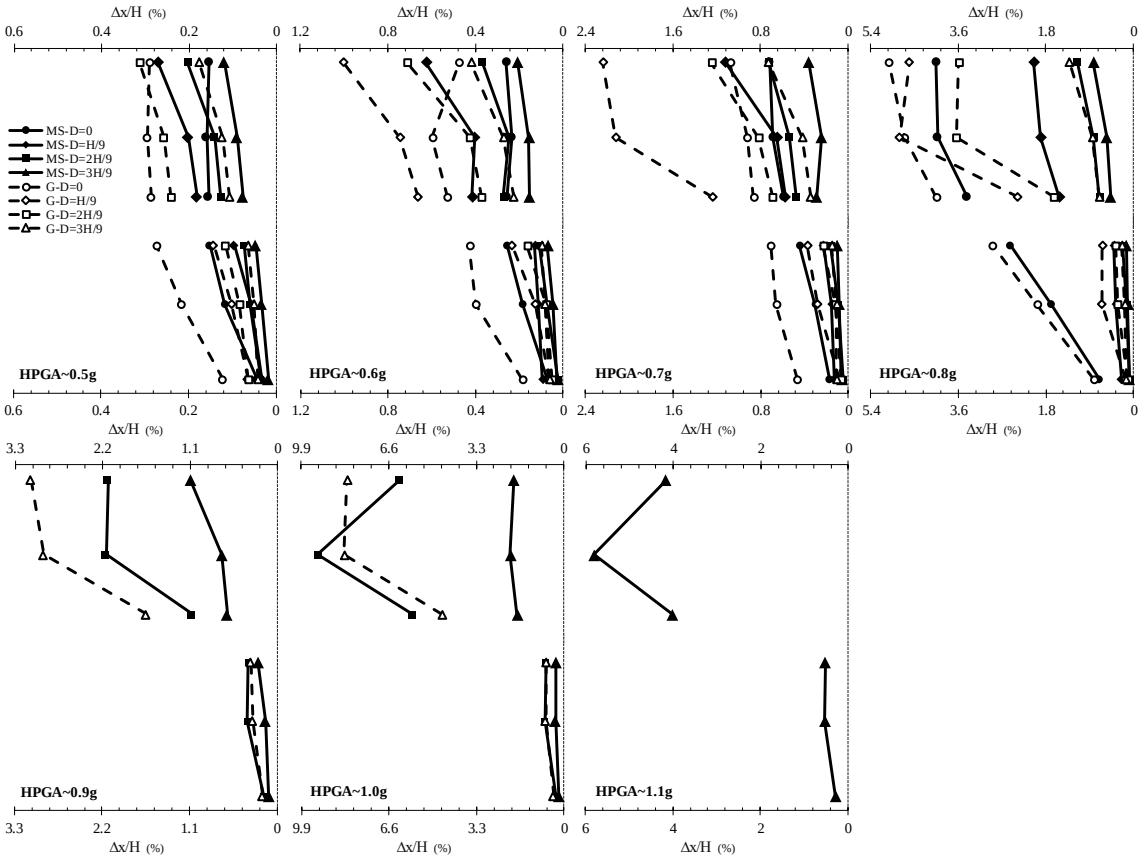

Fig. 7 Lateral displacement profiles under different base excitations

(1995) and Bathurst *et al*. (2012) stated that dynamic forces and dynamic pressure coefficients can be expressed as a combination of the initial static component and the dynamic increment component as follows

$$P_{AE} = P_A + \Delta P_{AE}, \quad P_{PE} = P_P + \Delta P_{PE} \tag{10}$$

$$K_{AE} = K_A + \Delta K_{AE}, \quad K_{PE} = K_P + \Delta K_{PE} \tag{11}$$

Therefore, the dynamic increment component of active force induced in retaining walls during a horizontal base excitation can be determine using the following equation

$$\Delta P_{AE} = \frac{1}{2}\Delta K_{AE}\gamma H^2 \tag{12}$$

In fact, ΔP_{AE} is equivalent to the active force mobilized in the models at each step of the seismic loading in the shaking table test.

3.1 Determination of k_h based on Mononobe-Okabe formulation

A back-calculation was made on M-O formulation to determine the horizontal pseudo static coefficient in the wall models. For this purpose, Eq. (12) was derived as follow

$$K_{AE} = \frac{\Delta P_{AE}}{\frac{1}{2}\gamma H^2} + K_A \tag{13}$$

Given the active force mobilized in the wall models is equal to the sum of maximum force increment mobilized in the reinforcements by shaking ($\Sigma\Delta T_{max,i}$) (Krishna and Latha 2009, Huang 2019, Xu *et al*. 2020), $\Sigma\Delta T_{max,i}$ can be substituted for ΔP_{AE} in Eq. (13) and k_h can be derived as a function of $\Sigma\Delta T_{max,i}$ as follows

$$\frac{cos^2(\varphi - tan^{-1}k_h)}{\cos(tan^{-1}k_h).\cos(\delta + tan^{-1}k_h)\left\{1 \pm \sqrt{\frac{\sin(\delta+\varphi).\sin(\varphi - tan^{-1}k_h)}{\cos(\delta + tan^{-1}k_h)}}\right\}^2} = \frac{\sum \Delta T_{max,i}}{\frac{1}{2}\gamma H^2} + \frac{cos^2(\varphi)}{\cos(\delta)\left\{1 \pm \sqrt{\frac{\sin(\delta+\varphi).\sin(\varphi)}{\cos(\delta)}}\right\}^2} \tag{14}$$

Thus, using Eq. (14) made it possible to determine k_h value for reinforced soil walls under horizontal seismic loading with specific mechanical properties based on the mobilized forces in the reinforcements.

3.2 k_h selection based on combination of shaking table results and M-O method

As seen in Eq. (14), the horizontal pseudo static coefficient in the wall models can be estimated by having the sum of maximum force increment mobilized in the reinforcements. Hence, by converting the values of $\Sigma\Delta T_{max,i}$ measured from shaking table tests to prototype scale ($(F)_{prototype} = N^2 (F)_{model}$) and substituting them in Eq. (14), the horizontal pseudo coefficient corresponding to HPGA

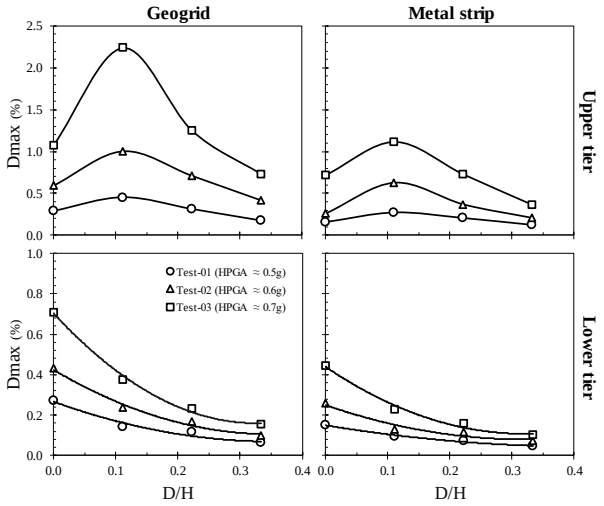

Fig. 8 Variation of maximum normalized deflection of the upper and lower tiers versus *D/H* ratio in different base accelerations

was determined for each wall models, separately. It should be noted that the force mobilized in the reinforcements, which were not instrumented, was estimated by interpolating the force of their upper and lower reinforcements. The variation of k_h versus HPGA in Fig. 9 shows an increasing trend as reported by other researchers.

The variation trend was such that a second order polynomial equation can be introduced to select k_h in all models as follow

$$k_h = \frac{HPGA}{g}\left(A_1 - B_1 \frac{HPGA}{g}\right) \quad (15)$$

where A_1 and B_1 are constant factors corresponding to the type of wall configuration and the reinforcement type, as presented in Table 4. This type of equation was also proposed by Segrestin and Bastick (1988) and El-Emam (2018) for geogrid-reinforced soil walls with full height rigid facing. As seen Fig. 9, the use of a tiered configuration reduced the required pseudo static coefficient. This reduction, which was observed in both reinforcement types, increased with increasing the offset distance but at a declining rate. This declining rate was more evident in the walls reinforced by geogrid. The reduction of the required pseudo static coefficient due to the use of geogrid instead of metal strips was another important point that was observed in Fig. 9. This k_h reduction, which was more prominent at $D \leq H/9$, highlights the need to simultaneously consider the reinforcement type and the offset distance in selecting the pseudo static coefficient. Slight reduction of k_h due to the use of geogrid at $D > 0.22H$ indicated that the effect of reinforcement type in selecting k_h can be ignored in these offset distances.

Comparison of k_h-HPGA variations obtained for the geogrid-reinforced models with those reported for geosynthetic-reinforced soil walls with full height rigid facing (Segrestin and Bastick 1988, El-Emam 2018) and wrap-around facing (Huang 2019) pointed to the influential role that the facing type played in selecting k_h. As seen in Fig. 9, the use of wrap-around facing, which is known as

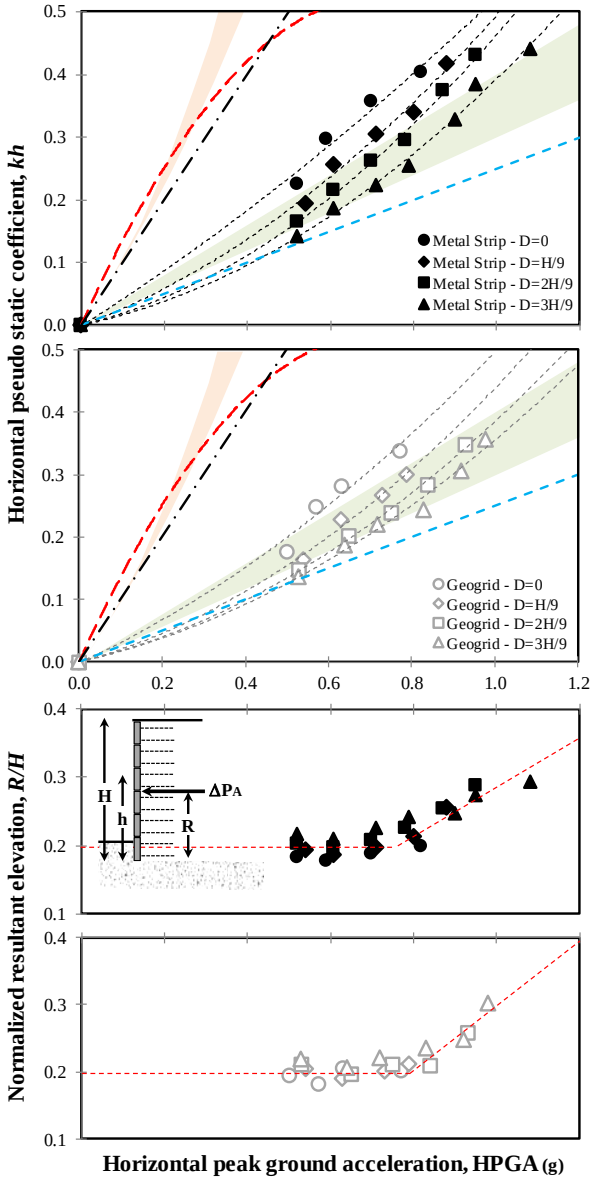

Fig. 9 Variation of k_h and position of resultant lateral force versus HPGA

the most flexible type of the facing in MSE walls, sharply reduced the required seismic coefficient. This reduction was so great that it made wrap-around reinforced soil walls one of the MSE walls with the lowest seismic coefficient required for analysis. On the other hand, comparison of the metal-strip reinforced models with geosynthetic-reinforced soil walls with full height rigid facing showed that the facing type had a much greater impact on k_h than the reinforcement type. As seen, despite the stiffer reinforcements in the metal-strip reinforced wall models, the required seismic coefficient in the walls with full height rigid facing was still higher. These observations point to the greater importance of paying attention to the facing type in selecting k_h than to the reinforcement type.

An accurate estimate of the location of the resultant force of incremental dynamic earth pressure (R) is the second important step in seismic analysis of retaining walls. $0.6H$ above the wall base was recommended by Seed and

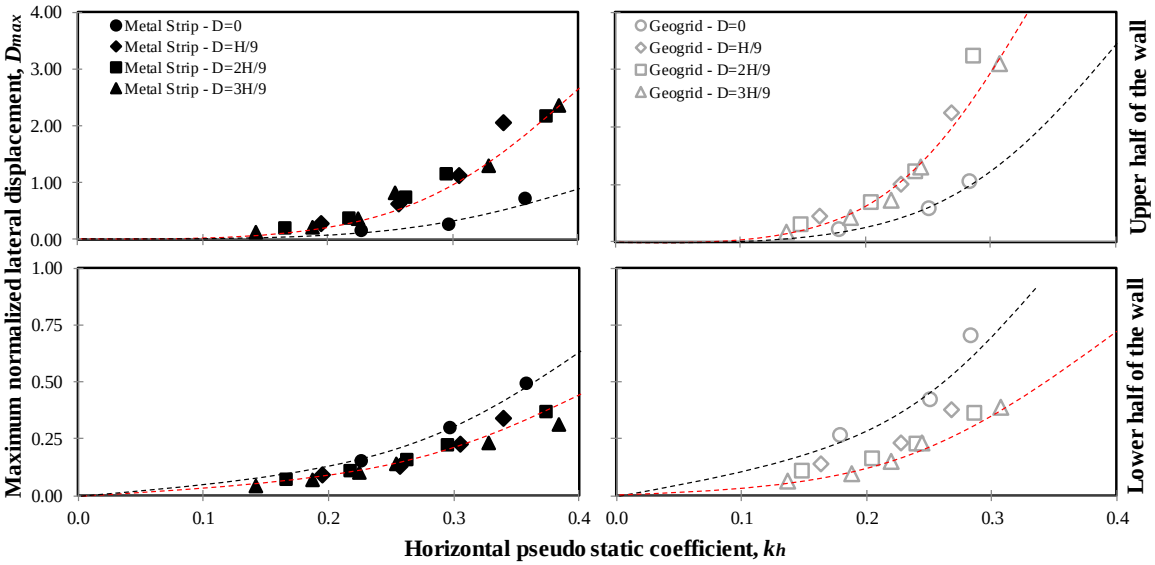

Fig. 10 Variation of maximum normalized lateral displacement versus k_h

Table 4 List of factors used in calculating k_h (Eq. (15))

Wall configuration	Reinforcement type	A_1	B_1
Integrated	Metal strip	0.4223	-0.1015
	Geogrid	0.3067	-0.1903
Two-tiered	Metal strip	$0.167D^{-0.251}$	$-0.126D^{-0.229}$
	Geogrid	$0.162D^{-0.214}$	$-0.117D^{-0.195}$

Whitman (1970) as the location of the resultant force of incremental dynamic earth pressure in gravity retaining walls and it is widely used in all types of earth walls. Using the obtained distribution of normalized lateral pressure increment along the wall height, R was calculated for all models at different values of HPGA. As seen in the variation of R versus HPGA in Fig. 9 for both reinforcements, R was estimated to be $0.2H$ at HPGA < 0.8g, while this was one third of that recommended for gravity retaining walls. This means that overturning mode is not in reinforced soil walls as probable as in gravity retaining walls under dynamic conditions and considering it as a potential deformation mode reduces design accuracy. R increased linearly with an increase in HPGA as reported by Woodward and Griffiths (1996) for gravity retaining walls and reached $0.35H$ and $0.4H$ at HPGA = 1.2 g in the metal-strip and geogrid wall models, respectively. Despite this increase, which occurred at very high base accelerations, the amount of R was still less than that recommended for gravity retaining walls. This finding indicates that even at very high base accelerations, using $R = 0.6H$ to analyze MSE walls can be far from the truth.

Wall displacement is used as the main criterion in evaluating the seismic performance of retaining walls. Because of its importance, numerous studies have been conducted to include the wall displacement as one of the criteria for selecting a pseudo-static coefficient in existing relationships. Most of these studies have focused on gravity retaining walls (Biondi *et al*. 2014, Macedo and Candia 2020, Lee *et al*. 2021) and little attention has been paid to MSE walls. Huang and Wang (2005) and Gaudio *et al*. (2018) are a few studies in which criteria have been proposed to select the pseudo-static coefficient based on the wall displacement. These criteria are very general and have been provided regardless of important factors such as wall configuration, reinforcement type, etc.

To provide a more comprehensive criterion for selecting k_h based on the wall displacement in which the effect of the reinforcement type and the wall configuration be also considered, it was attempted to find a relationship between pseudo-static coefficients calculated for the models and the displacement recorded for them during the shaking table tests. For this purpose, the variation of maximum normalized lateral displacement (D_{max}) versus k_h is presented in Fig. 10 for the upper and lower halves of the models, separately. As can be seen, there is a nonlinear relationship between D_{max} and k_h in the tiered and integrated wall models, which can be well expressed as a power equation with a high correlation coefficient as follow

$$D_{max} = A_2(k_h)^{B_2} \tag{16}$$

Based on Eq. (16), the horizontal pseudo-static coefficient can be selected based on the expected level of performance. Providing Eq. (16) for the upper and lower half of the wall separately makes it possible to select k_h for each part of the wall in proportion to the displacement occurred in it. This will optimize the analysis and therefore the design. By comparing the variation of D_{max} versus k_h for different reinforcements in Fig. 10, an increasing trend was observed in D_{max} with an increase in horizontal pseudo-static coefficient. The rate of D_{max} growth in the geogrid-reinforced soil models was higher than the metal-strip reinforced-soil walls. This means that when using extensible reinforcements instead of inextensible ones, a lower pseudo-static coefficient should be used for analysis to prevent the wall performance level from changing. This finding, which was true for both integrated and tiered walls, is an emphasis on considering the reinforcement type in

Table 5 List of factors used in calculating k_h based on the wall displacement (Eq. (16))

Wall configuration	Reinforcement type	Upper half of the wall		Lower half of the wall	
		A_2	B_2	A_2	B_2
Integrated	Metal strip	17.74	3.27	7.03	2.59
	Geogrid	62.08	3.27	7.10	1.91
Two-tiered	Metal strip	40.89	2.99	3.39	2.25
	Geogrid	194.65	3.59	5.77	2.33

calculating the pseudo static coefficient of reinforced soil walls. Because the acceleration criterion (Eq. (15)) and the displacement criterion (Eq. (16)) will not necessarily provide the same k_h and the pseudo-static coefficient should not be chosen in the absence of a design earthquake, the acceleration and displacement criteria should be considered as the main and control criterion in the selection of k_h. This was also suggested by other researchers (Biondi *et al*. 2014, Huang and Wang 2005).

5. Conclusions

In the current study, it was attempted to introduce the horizontal pseudo static coefficient (k_h) for of reinforced soil walls as a function of wall configuration and reinforcement type for use in Mononobe-Okabe method. For this purpose, eight reduced-scale shake table tests were performed on integrated and two-tiered wall models reinforced by metal strip and geogrid to determine the distribution of tensile force along the reinforcements and the dynamic lateral pressure in the models. Tiered wall models were prepared with three offset distances (D=H/9, 2H/9 and 3H/9) to also take into account the effect of the offset distance in selecting k_h. Then, the physical models were analyzed using Mononobe-Okabe method to estimate the value of k_h required to establish the dynamic lateral pressures similar to those observed in the shaking table tests. Based on the results, k_h and the position of resultant lateral force (R) were introduced as a function of the horizontal peak ground acceleration (HPGA), the offset distance as well as the reinforcement type and also were compared with those reported by other studies. Moreover, a displacement criterion was also introduced to select k_h based on the observed deformations from the shaking table tests. The following points summarize the major findings of this research:

- Matching the failure surfaces obtained from particle image velocimetry (PIV) with the force distribution in the reinforcements showed that the maximum force (T_{max}) will be approximately mobilized at the intersection of the failure surface with the reinforcements if the failure plane can be formed, otherwise T_{max} is mobilized at reinforcements' head.
- PIV results showed that the use of a tiered configuration in the reinforced soil walls, even with a small offset distance (D = H/9), prevented the failure surface from developing in the lower tier and led to this part of the wall experienced only a simple shear deformation along horizontal planes.
- The reduction in reinforcement load, which was accompanied by a change in the failure geometry from concave to convex in the lower half of the integrated walls and the formation of a secondary failure surface in the upper half of the tiered walls, was observed due to the use of geogrid in the models.
- *0.22H* was identified as the minimum offset distance required to prevent excess movement when constructing reinforced soil walls in a tiered configuration. It was also found that at offset distances greater than this value, the effect of reinforcement type in calculating k_h can be ignored.
- Comparison of results with those reported in other studies showed that the effect of facing type on k_h was much greater than the reinforcement type.
- Determining 0.2H as the location of the resultant force of incremental dynamic earth pressure (R) for both reinforcement types indicated that overturning mode is not in reinforced soil walls as probable as in gravity retaining walls at HPGA < 0.8 g. This probability increased with increasing R up to 0.35H and 0.4H at HPGA = 1.2 g in the metal-strip and geogrid wall models, respectively.
- The variation of maximum normalized lateral displacement (D_{max}) versus k_h indicated that to prevent the wall performance level from changing, a lower pseudo-static coefficient should be used for analysis when using extensible reinforcements instead of inextensible ones.

Acknowledgments

The authors would like to thank of Prof. R.J. Bathurst, Prof. A. Ghalandarzade and Mr. M.A. Salimi for providing valuable assistance and also gratefully appreciate the support of the Centrifuge and Physical Modeling Center at Tehran University.

References

Allen, T.M. Bathurst, R.J. (2014). "Performance of a 11 m high block-faced geogrid wall designed using the K-stiffness method", *Can. Geotech. J.*, **51**(1), 16-29. https://doi.org/10.1139/cgj-2013-0261.

Altay, G., Kayadelen, C., Canakci, H., Bagriacik, B., Ok, B. and Oguzhanoglu, M.A. (2021), "Experimental investigation of deformation behavior of geocell retaining walls", *Geomech. Eng.*, **27**(5), 419-431.

https://doi.org/10.12989/gae.2021.27.5.419.

Bathurst, R.J. (1990), "Instrumentation of geogrid-reinforced soil wall", *Transport. Res. Record*, **1277**, 102-111.

Bathurst, R.J. and Cai, Z. (1995), "Pseudo-static analysis of geosynthetic-reinforced segmental retaining walls", *Geosynth. Int.*, **2**(5), 787-830. https://doi/abs/10.1680/gein.2.0037.

Bathurst, R.J., Hatami, K. and Alfaro, M.C. (2012), Geosynthetic reinforced soil walls and slopes-seismic aspects. Handbook of Geosynthetic Engineering, Shukla, SK.

Bathurst, R.J. and Hatami, K. (2020), "Earthquake response analysis of reinforced-soil walls using FLAC", *In Flac and Numerical Modeling in Geomechanics CRC Press*.

Bathurst, R.J. and Naftchali, F.M. (2021), "Geosynthetic reinforcement stiffness for analytical and numerical modelling of reinforced soil structures", *Geotext. Geomembranes*, **49**(4), 921-940. https://doi.org/10.1016/j.geotexmem.2021.01.003.

Biondi, G., Cascone, E. and Maugeri, M. (2014), "Displacement versus pseudo-static evaluation of the seismic performance of sliding retaining walls", *Bull. Earthq. Eng.*, **12**(3), 1239-1267. https://doi.org/10.1007/s10518-013-9542-4.

Cai, Z. and Bathurst, R.J. (1995), "Seismic response analysis of geosynthetic reinforced soil segmental retaining walls by finite element method", *Comput. Geotech.*, **17**(4), 523-546. https://doi.org/10.1016/0266-352X(95)94918-G.

CEN (2004), "EN 1998-5: Eurocode 8: Design of structures for earthquake resistance. Part 5: foundations, retaining structures and geotechnical aspects", Brussels, Belgium.

Choukeir, M. (1995), "Finite element analysis of reinforced earth and soil nailed structures under seismic loading", PhD thesis, Polytechnic University, New York.

El-Emam, M.M. (2018), "Experimental verification of current seismic analysis methods of reinforced soil walls", *Soil Dyn. Earthq. Eng.*, **113**, 241-255. https://doi.org/10.1016/j.soildyn.2018.06.006.

FHWA (2009), "Design and Construction of Mechanically Stabilized Earth Walls and Reinforced Soil Slopes – Volume I, Federal Highway Administration Publication No. FHWA-NHI-10-243", US Department of Transportation, Washington, DC, USA.

Gaudio, D., Masini, L. and Rampello, S. (2018), "A performance-based approach to design reinforced-earth retaining walls", *Geotext. Geomembranes*, **46**(4), 470-485. https://doi.org/10.1016/j.geotexmem.2018.04.003.

Hatami, K. and Bathurst, R.J. (2000), "Effect of structural design on fundamental frequency of reinforced-soil retaining walls" *Soil Dyn. Earthq. Eng.*, **19**(3), 137-157. https://doi.org/10.1016/S0267-7261(00)00010-5.

Hosseininia, H. and Ashjaee, A. (2018), "Numerical simulation of two-tier geosynthetic-reinforced-soil walls using two-phase approach", *Comput. Geotech.*, **100**, 15-29. https://doi.org/10.1016/j.compgeo.2018.04.003.

Huang, C.C. and Wang, W.C. (2005), "Seismic displacement charts for the performance-based assessment of reinforced soil walls", *Geosynth. Int.*, **12(4)**, 176-190. https://doi/10.1680/gein.2005.12.4.176.

Huang, C.C. (2016), "Settlement of footings at the crest of reinforced slopes subjected to toe unloading", *Geosynth. Int.*, **23**(4), 247-256. https:// doi/10.1680/jgein.15.00045.

Huang, C.C. (2019), "Seismic responses of vertical-faced wrap-around reinforced soil walls", *Geosynth. Int.*, **26**(2), 146-163. https:// doi/abs/10.1680/jgein.18.00044.

Hong, Y.S., Chen, R.H., Wu, C.S. and Chen, J.R. (2005), "Shaking table tests and stability analysis of steep nailed slopes", *Can. Geotech. J.*, **42**(5), 1264-1279. https://doi.org/10.1139/T05-055.

Iai, S. (1989), "Similitude for shaking table tests on soil-structure-fluid model in 1g gravitational field", *Soils Found.*, **29**(1), 105-118. https://doi.org/10.3208/sandf1972.29.105.

Jamnani, A.R., Yazdandoust, M. and Sabermahani, M. (2023), "Effect of a two-tiered configuration on the seismic behaviour of reinforced soil walls", *Geosynth. Int.*, **30**(1), 3-28. https://doi.org/10.1680/jgein.22.00150.

Jiang, Y., Han, J., Parsons, R.L. and Brennan, J.J. (2016), "Field instrumentation and evaluation of modular-block MSE walls with secondary geogrid layers", *J. Geotech. Geoenviron. Eng.*, **142**(12), 05016002. https://doi.org/10.1061/(ASCE)GT.1943-5606.0001573.

Jin, H., Zhang, G. and Yang, Y. (2021), "Experimental and numerical study on behavior of retaining structure with limited soil", *Geomech. Eng.*, **26**(1), 77-88. https://doi.org/10.12989/gae.2021.26.1.077.

Kahyaoglu, M.R. and Sahin, M. (2021), "Model studies on polymer strip reinforced soil retaining walls", *Geomech. Eng.*, **25**(5), 357-371. https://doi.org/10.12989/gae.2021.25.5.357.

Komak Panah, A., Yazdi, M. and Ghalandarzadeh, A. (2015), "Shaking table tests on soil retaining walls reinforced by polymeric strips", *Geotext Geomembranes*, **43**(2), 148-161. https://doi.org/10.1016/j.geotexmem.2015.01.001.

Kongkitkul, W., Tatsuoka, F., Hirakawa, D., Sugimoto, T., Kawahata, S. and Ito, M. (2010), "Time histories of tensile force in geogrid arranged in two full-scale high walls", *Geosynth. Int*., **17**(1), 12-32. https://doi.org/10.1680/gein.2010.17.1.12.

Koseki, J., Tatsuoka, F., Munaf, Y., Tateyama, M. and Kojima, K. (1998), "A modified procedure to evaluate active earth pressure at high seismic loads", *Soils Found.*, **38**, 209-216. https://doi.org/10.3208/sandf.38.Special_209.

Krishna, A.M. and Latha, G.M. (2009), "Seismic behavior of rigid-faced reinforced 567 soil retaining wall models: reinforcement effect", *Geosynth. Int.*, **16**(5), 364-373. https:// doi/abs/10.1680/gein.2009.16.5.364.

Krishna, A.M. and Latha, G.M. (2011), "Modeling the dynamic response of wrap-faced reinforced soil retaining walls", *Int. J. Geomech*., **12**(4), 439-450. https://doi.org/10.1061/(ASCE)GM.1943-5622.0000128.

Kramer, S.L. (1996), "Geotechnical earthquake engineering", Prentice-Hall, Upper Saddle River, NJ.

Kumar, J. and Rao, K.S. (1997), "Passive pressure coefficients, critical failure surface and its kinematic admissibility", *Geotechnique*, **47**(1), 185-192. https://doi.org/10.1680/geot.1997.47.1.185.

Leshchinsky, D., Ling, H.I., Wang, J.P., Rosen, A. and Mohri, Y. (2009), "Equivalent seismic coefficient in geocell retention systems", *Geotext. Geomembranes*, **27**(1), 9-18. https://doi.org/10.1016/j.geotexmem.2008.03.001.

Lee, M.G., Ha, J.G., Jo, S.B., Park, H.J. and Kim, D.S. (2017), "Assessment of horizontal seismic coefficient for gravity quay walls by centrifuge tests", *Géotechnique Lett.*, **7**(2), 211-217. https:// doi/pdf/10.1680/jgele.17.00005.

Lee, M.G., Ha, J.G., Cho, H.I., Sun, C.G. and Kim, D.S. (2021), "Improved performance-based seismic coefficient for gravity-type quay walls based on centrifuge test results", *Acta Geotechnica*, **16**(4), 1187-1204. https://doi.org/10.1007/s11440-020-01086-5.

Lee, S.W. (2019), "Experimental study on effect of underground excavation distance on the behavior of retaining wall", *Geomech. Eng.*, **17**(5), 413-420. https://doi.org/10.12989/gae.2019.17.5.413.

Li, F.L., Ma, T.R. and Yang, Y.G. (2021), "Numerical study on the rate-dependent behavior of geogrid reinforced sand retaining walls", *Geomech. Eng.*, **25**(3), 195-205. https://doi.org/10.12989/gae.2021.25.3.195.

Liu, H., Yang, G. and Ling, H.I. (2014), "Seismic response of multi-tiered reinforced soil retaining walls", *Soil Dyn. Earthq.*

Eng., **61**, 1-12. https://doi.org/10.1016/j.soildyn.2014.01.012.
Mollaei, R., Yazdandoust, M. and Askari, F. (2022), "Seismic evaluation of helical soil-nailed walls using shaking table testing", *Soil Dyn. Earthq. Eng.*, **163**, 107331. https://doi.org/10.1016/j.soildyn.2022.107331.
Maced, J. and Candia, G. (2020), "Performance-based assessment of the seismic pseudo-static coefficient used in slope stability analysis", *Soil Dyn. Earthq. Eng.*, **133**, 106109. https://doi.org/10.1016/j.soildyn.2020.106109.
MOF (2014), "Ports and fishing harbours design code", Sejong, Korea: Ministry of Oceans and Fisheries (in Korean).
Safa, M., Maleka, A., Arjomand, M.A., Khorami, M. and Shariati, M. (2019), "Strain rate effects on soil-geosynthetic interaction in fine-grained soil", *Geomech. Eng.*, **19**(6), 533-542. https://doi.org/10.12989/gae.2019.19.6.533.
Safaee, A.M., Mahboubi, A. and Noorzad, A. (2021), "Experimental investigation on the performance of multi-tiered geogrid mechanically stabilized earth (MSE) walls with wrap-around facing subjected to earthquake loading", *Geotext. Geomembranes*, **49**(1), 130-145. https://doi.org/10.1016/j.geotexmem.2020.08.008.
Samee, A.A., Yazdandoust, M. and Ghalandarzadeh, A. (2021), "Performance of back-to-back MSE walls reinforced with steel strips under seismic conditions", *Transport. Geotech.*, **30**, 100540. https://doi.org/10.1016/j.trgeo.2021.100540.
Samee, A.A., Yazdandoust, M. and Ghalandarzadeh, A. (2022), "Effect of reinforcement arrangement on dynamic behaviour of back-to-back mechanically stabilised earth walls", *Int. J. Phys. Model. Geotech.*, **22**(4), 208-223. https://doi.org/10.1680/jphmg.20.00088.
Seed, H.B. and Whitman, R.V. (1970), "Design of earth retaining structures for dynamic loads", *Proceedings of the special conference on lateral stresses in the ground and design of earth retaining structures*.
Segrestin, P. and Bastick, M.J. (1988), "Seismic design of reinforced earth retaining walls: the contribution of finite element analysis", *Proceedings of the Int. Symp. on Theory and Practice of Earth Reinforcement*, Kyushu, Japan.
Seo, S., Lim, H. and Chung, M. (2021), "Evaluation of failure mode of tunnel-type anchorage for a suspension bridge via scaled model tests and image processing", *Geomech. Eng.*, **24**(5), 457-470. https://doi.org/10.12989/gae.2021.24.5.457.
Stuedlein, A.W., Bailey, M.J., Lindquist, D.D., Sankey, J. and Neely, W.J. (2010), "Design and performance of a 46-m-high MSE wall", *J. Geotech. Geoenviron. Eng.*, **136**(6), 786-796. https://doi.org/10.1061/(ASCE)GT.1943-5606.0000294.
Tatsuoka, F., Munoz, H., Kuroda, T., Nishikiori, H., Soma, R., Kiyota, T. and Watanabe, K. (2012), "Stability of existing bridges improved by structural integration and nailing", *Soils Found.*, **52**(3), 430-448. https://doi.org/10.1016/j.sandf.2012.05.004.
Tufenkjian, M.R. and Vucetic, M. (2000), "Dynamic failure mechanism of soil-nailed excavation models in centrifuge", *J. Geotech. Geoenviron. Eng.*, **126**(3), 227-235. https://doi.org/10.1061/(ASCE)1090-0241(2000)126:3(227).
Viswanadham, B.V.S. and König, D. (2004), "Studies on scaling and instrumentation of a geogrid", *Geotextiles Geomembranes*, **22**(5), 307-328. https://doi.org/10.1016/S0266-1144(03)00045-1.
Viswanadham, B.V.S. and Mahajan, R.R. (2007), "Centrifuge model tests on geotextile-reinforced slopes", *Geosynth. Int.*, **14**(6), 365-379. https:// doi/abs/10.1680/gein.2007.14.6.365.
Watanabe, K., Munaf, Y., Koseki, J., Tateyama, M. and Kojima, K. (2003), "Behavior of several types of model retaining walls subjected to irregular excitation", *Soils Found.*, **43**(5), 13-27. https://doi.org/10.3208/sandf.43.5_13.
White, D. and Take, A. (2002), "GeoPIV: Particle Image Velocimetry (PIV) software for use in geotechnical testing", PhD thesis, University of Cambridge, Cambridge, UK.
Won, M.S., Lee, O., Kim, Y.S. and Choi, S.K. (2016), "A 12-year long-term study on the external deformation behavior of Geosynthetic Reinforced Soil (GRS) walls", *Geomech. Eng.*, **10**(5), 565-575. https://doi.org/10.12989/gae.2016.10.5.565.
Woodward, P.K. and Griffiths, D.V. (1996), "Comparison of the pseudo-static and dynamic behavior of gravity retaining walls", *Geotech. Geol. Eng.*, **14**(4), 269-290. https://doi.org/10.1007/BF00421944.
Wood, D.M. (2004), "Geotechnical modeling", Version 2.2. London: Taylor & Francis Group.
Xu, P., Hatami, K. and Jiang, G. (2020), "Shaking table study of the influence of facing on reinforced soil wall connection loads", *Geosynth. Int.*, **27**(4), 364-378. https://doi/full/10.1680/jgein.20.00001.
Yadegari, S., Yazdandoust, M. and Momeniyan, M. (2023), "Performance of helical soil-nailed walls under bridge abutment", *Transport. Geotechnics*, **38**, 100788. https://doi.org/10.1016/j.trgeo.2022.100788.
Yazdandoust, M. (2017), "Investigation on the seismic performance of steel-strip reinforced-soil retaining walls using shaking table test", *Soil Dyn. Earthq. Eng.*, **97**, 216-232. https://doi.org/10.1016/j.soildyn.2017.03.011.
Yazdandoust, M. (2018), "Laboratory evaluation of dynamic behavior of steel-strip mechanically stabilized earth walls", *Soils Found.*, **58**(2), 264-276. https://doi.org/10.1016/j.sandf.2018.02.016.
Yazdandoust, M., Ghalandarzadeh, A. (2020), "Pseudo-static coefficient in reinforced soil structures". *Int. J. Phys. Model. Geotech.*, **20**(6), 320-337.
Yazdandoust, M. and Bahrami, A. (2022), "Performance of two-tiered reinforced-soil retaining walls under strip footing load", *Geotext. Geomembranes*, **50**(4), 545-565. https://doi.org/10.1016/j.geotexmem.2020.04.002.
Yazdandoust, M., Samee, A.A. and Ghalandarzadeh, A. (2022), "Assessment of seismic behavior of back-to-back mechanically stabilized earth walls using 1g shaking table tests", *Soil Dyn. Earthq. Eng.*, **155**, 106078. https://doi.org/10.1016/j.soildyn.2020.106078.
Yoshida, T. and Tatsuoka, F. (1990), "Deformation property of shear band in sand subjected to plane strain compression and its relation to particle characteristics", *Proceedings of the 12th Int. Conf. Soil Mech. Found. Engng*, Rio de Janeiro.
Yoo, C. and Kim, S.B. (2008), "Performance of a two-tier geosynthetic reinforced segmental retaining wall under a surcharge load: full-scale load test and 3D finite element analysis". *Geotext Geomembranes*, **26**(6), 447518. https://doi.org/10.1016/j.geotexmem.2008.05.008.
Yoo, C. (2018), "Serviceability state deformation behaviour of two-tiered geosynthetic reinforced soil walls", *Geosynth. Int.*, **25**(1), 12–25. https:// doi/10.1680/jgein.17.00030.
Zarnani, S., El-Emam, M.M. and Bathurst, R.J. (2011), "Comparison of numerical and analytical solutions for reinforced soil wall shaking table tests", *Geomech. Eng.*, **3**(4), 291-321. https://doi.org/10.12989/gae.2011.3.4.291.

CC